Numerical Investigation of a Two-Phase Nanofluid Model for Boundary Layer Flow Past a Variable Thickness Sheet

Liu, Chunyan; Zheng, Liancun; Lin, Ping; Pan, Mingyang; Liu, Fawang

Published in:
Zeitschrift fur Naturforschung A: a Journal of Physical Sciences

DOI:
10.1515/zna-2017-0372

Publication date:
2018

Document Version
Peer reviewed version

Numerical investigation of a two-phase nanofluid model for boundary layer flow past a variable thickness sheet

Chunyan Liu[a,b], Liancun Zheng[a,b,*], Ping Lin[a,c], Mingyang Pan[d], Fawang Liu[e]

[a] *School of Mathematics and Physics, University of Science and Technology Beijing, Beijing 100083, China*
[b] *Beijing Key Laboratory for Magneto-Photoelectrical Composite and Interface Science, Beijing 100083, China*
[c] *Division of Mathematics, University of Dundee, Dundee DD1 4HN, Scotland, United Kingdom*
[d] *School of Energy and Environmental Engineering, University of Science and Technology Beijing, Beijing 100083, China*
[e] *School of Mathematical Sciences, Queensland University of Technology, GPO Box 2434, Brisbane, QLD. 4001, Australia*

Abstract

This paper investigates heat and mass transfer of nanofluid over a stretching sheet with variable thickness. The techniques of similarity transformation and homotopy analysis method (HAM) are used to find solutions. Velocity, temperature and concentration fields are examined with the variations of governing parameters. Local Nusselt number and Sherwood number are compared for different values of variable thickness parameter. Results show that there exists a critical value of thickness parameter β_c ($\beta_c \approx 0.7$) where the Sherwood number achieves its maximum at the critical value β_c. For $\beta > \beta_c$, the distribution of nanoparticle volume fraction decreases near the surface but exhibits an opposite trend far from the surface.

Keywords: Nanofluid, Two-phase mixture model, Variable thickness surface, Homotopy analysis method

*Corresponding author.Tel.:+86(10)6233 2002
Email address: liancunzheng@ustb.edu.cn (Liancun Zheng)

1. Introduction

Nanofluid has been the topic of extensive research owing to its excellent physical properties especially high thermal conductivity [1–3]. Boungiorno [4] demonstrated that the Brownian diffusion and thermophoresis are the two most important mechanisms to account for the abnormal convective heat transfer enhancement in nanofluid. On the basis of these analyses, a new two-component four-equation model of the conservation of mass, momentum, and heat transport in nanofluid was proposed. From then on, a lot of scholars have studied this model to perform the effects of Brownian diffusion and thermophoresis in different systems [5–9]. Kuznetsov and Nield [10] considered natural convective boundary-layer flow of nanofluid past a vertical plate. Sheikholeslami et al. [11] investigated the natural convection heat transfer of nanofluid in an enclosure under magnetic field numerically. Eid and Mahny [12] focused on heat and mass transfer of a non-Newtonian nanofluid flow described by a two-phase model, see also [13–17] for related works.

The boundary layer flow past a stretching sheet has attracted considerable attention in many fields of industry and engineering processes. Its applications appear in melt-spinning, manufacture of plastic and rubber sheets, etc. Rollins and Vajravelu [18] studied heat transfer characteristics of a second-order fluid over a stretching sheet with linearly varying velocity. Khan and Pop [19] investigated heat and mass transfer of nanofluid driven by a linear stretching sheet and the effects of Brownian motion and thermophoresis were considered. The investigations of laminar flow of a nanofluid over a stretching sheet with a convective boundary condition [20]. However, the motion of the sheet may not necessarily be linear. Ali [21] analyzed the flow and heat transfer which is driven by a power-law stretched surface subject to suction or injection. Further, the study of boundary layer flow and heat transfer was extended to an exponentially stretching sheet by Magyari and Keller [22]. Moreover, the stretching sheet with variable thickness was proposed by Fang et al. due to its practical importance [23]. In that investigation, they had shown that the non-flat

stretching sheet influences the boundary layer development along the wall and the shear stress distribution in the fluid. Subsequently, a number of researches have been conducted to examine the thickness-varying stretching sheet in Refs. [24–27]. To the best of our knowledge, investigation of exponential stretching sheet considering variable thickness in current literatures is still lacking. Therefore, the objective of this paper is to study the boundary layer flow, heat and mass transfer of Maxwell nanofluid over an exponential stretching sheet with variable thickness.

In view of fluid diversity in nature, the generalized Maxwell constitutive equation with upper-convected derivative has been widely studied to describe viscoelastic properties of non-Newtonian fluid. This type of constitutive relation includes the relaxation time effects. Sadeghy et al. [28] investigated laminar flow of the upper-convected Maxwell (UCM) model over a moving rigid plate. They found that the skin friction decreases with increasing the Deborah number. The unsteady flow of Maxwell fluid between two side walls induced by a suddenly moving wall was studied by Hayat et al. [29]. Singh and Agarwal [30] reported the effects of variable viscosity and variable thermal conductivity on the steady flow and heat transfer of Maxwell fluid. The results indicated that the skin friction and heat transfer coefficient are lower for the Maxwell fluid than constant viscosity and thermal conductivity coefficient. Recently, Hsiao [31] investigated the applications of Maxwell fluid in extrusion manufacturing processing. By improved parameters control method, he found that the larger Schmidt number will produce the higher mass transfer effects. Finally, we mention a few interesting problems studied by different scholars in this field [32–34].

The homotopy analysis method (HAM) is an analytic approximation method for solving nonlinear equations introduced by Liao in 1992 [35] and the effectiveness of the HAM has been validated by himself [36] and other scholars [37, 38]. This method has got extensive successful results by solving many types of nonlinear equations in science and engineering [39, 40]. In this paper, HAM is applied to solve the reduced governing equations resulting from the similarity transformation. The paper is organized as follows: in Section 2, the mathe-

matical model is formulated. The detailed similarity reduction procedures for the governing equations are presented in Section 3. The analyses of results and discussions are given in Section 4, followed by conclusions in Section 5.

2. Mathematical formulation of the physical model

Consider a two-dimensional steady laminar flow of viscoelastic incompressible Maxwell nanofluid over an exponential stretching sheet with variable thickness in the form of $y = ae^{-nx/2l}$, $(a > 0, n > 0)$. Note that for $n = 0$ the stretching surface is of same thickness. It is assumed that the motion of the extendable sheet satisfies the velocity distribution $U_w(x) = u_0 V(x)$ [41], where $V(x) = e^{nx/l}$. The ambient temperature and nanoparticle volume fraction are T_∞ and C_∞. The temperature T and nanoparticle volume fraction C on the wall are denoted as $T_w(x) = T_\infty + T_0 V(x/2)$ and $C_w(x) = C_\infty + C_0 V(x/2)$, respectively. It is assumed that the horizontal velocity is slow, with negligible effect on the distribution of temperature and nanoparticle volume fraction. The physical model and coordinate system are shown in Fig. 1. The boundary layer equations governing the conservations of fluid mass, momentum, energy and nanoparticle mass can be expressed as follows

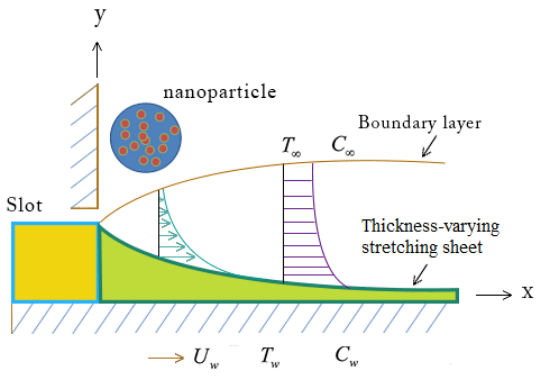

Fig. 1: The physical model of a stretching sheet with variable thickness.

$$\frac{\partial u}{\partial x}+\frac{\partial v}{\partial y}=0, \tag{1}$$

$$u\frac{\partial u}{\partial x}+v\frac{\partial u}{\partial y}+\lambda_1\left(u^2\frac{\partial^2 u}{\partial x^2}+2uv\frac{\partial^2 u}{\partial x\partial y}+v^2\frac{\partial^2 u}{\partial y^2}\right)=\nu\frac{\partial^2 u}{\partial y^2}, \tag{2}$$

$$u\frac{\partial T}{\partial x}+v\frac{\partial T}{\partial y}=\alpha\frac{\partial^2 T}{\partial y^2}+\tau\left[D_B\left(\frac{\partial C}{\partial y}\frac{\partial T}{\partial y}\right)+\frac{D_T}{T_\infty}\left(\frac{\partial T}{\partial y}\right)^2\right], \tag{3}$$

$$u\frac{\partial C}{\partial x}+v\frac{\partial C}{\partial y}=D_B\frac{\partial^2 C}{\partial y^2}+\frac{D_T}{T_\infty}\frac{\partial^2 T}{\partial y^2}. \tag{4}$$

The boundary conditions are:

$$\begin{aligned} y=ae^{-\frac{nx}{2l}}&:u=U_w(x),v=0,T=T_w(x),C=C_w(x)\\ y\to\infty&:u\to 0,v\to 0,T\to T_\infty,C\to C_\infty, \end{aligned} \tag{5}$$

where u and v are velocity components in the directions of x and y, λ_1 is the relaxation time parameter, ν is the coefficient of kinematic viscosity. α is the coefficient of thermal diffusivity of the fluid, D_B is the Brownian diffusion coefficient, D_T is the thermophoretic diffusion coefficient and $\tau=(\rho c_p)_p/(\rho c_p)_f$ is the ratio between the effective heat capacity of the nanoparticle and heat capacity of the fluid. a is a positive variable thickness parameter, n is the exponential shape parameter and l is the reference length. The u_0 is a reference velocity. T_0 and C_0 are reference temperature and reference nanoparticle volume fraction in the stretching sheet.

3. Nonlinear boundary value problems

Let ψ be the stream function satisfying $u=\partial\psi/\partial y, v=-\partial\psi/\partial x$. Introduce the following dimensionless functions F, θ, ϕ and the similarity variable η as [7, 42]

$$\begin{aligned} &\eta=\sqrt{\frac{u_0}{2\nu l}}V(\frac{x}{2})y,\psi=\sqrt{2\nu l u_0}F(\eta)V(\frac{x}{2}),v=-n\sqrt{\frac{\nu u_0}{2l}}V(\frac{x}{2})(F(\eta)+\eta F'(\eta)),\\ &u=u_0V(x)F'(\eta),T=T_\infty+T_0V(\frac{x}{2})\theta,C=C_\infty+C_0V(\frac{x}{2})\phi, \end{aligned} \tag{6}$$

substituting Eq. (6) into Eqs. (1)-(4), then the following nonlinear ordinary differential equations are obtained

$$F''' - 2nF'^2 + nFF'' + \lambda n^2(3FF'F'' + \frac{1}{2}\eta F'^2F'' - \frac{1}{2}F^2F''' - 2F'^3) = 0, \quad (7)$$

$$\frac{1}{Pr}\theta'' + nF\theta' + Nb\theta'\phi' + Nt\theta'^2 = 0, \quad (8)$$

$$\phi'' + nScF\phi' + \frac{Nt}{Nb}\theta'' = 0, \quad (9)$$

and the boundary conditions (5) are converted into

$$F(\beta) = -\beta, F'(\beta) = 1, \theta(\beta) = 1, \phi(\beta) = 1, \quad (10)$$

$$F'(\infty) = 0, \theta(\infty) = 0, \phi(\infty) = 0, \quad (11)$$

with the associated parameters, here primes denote differentiation with respect to η. $\beta = \eta = a\sqrt{u_0/2\nu l}$ is the surface thickness parameter. To facilitate the computation, the coordinate transform $\xi = \eta - \beta$ is exploited. The Eqs. (7)-(9) and the associated boundary conditions (10)-(11) become

$$f''' - 2nf'^2 + nff'' + \lambda n^2(3ff'f'' + \frac{1}{2}(\xi + \beta)f'^2f'' - \frac{1}{2}f^2f''' - 2f'^3) = 0, \quad (12)$$

$$\frac{1}{Pr}\theta'' + nf\theta' + Nb\theta'\phi' + Nt\theta'^2 = 0, \quad (13)$$

$$\phi'' + nScf\phi' + \frac{Nt}{Nb}\theta'' = 0, \quad (14)$$

$$f(0) = -\beta, f'(0) = 1, \theta(0) = 1, \phi(0) = 1, \quad (15)$$

$$f'(\infty) = 0, \theta(\infty) = 0, \phi(\infty) = 0, \quad (16)$$

where $\lambda > 0$ is the local Deborah number, Pr is the Prandtl number, Sc is the Schmidt number, β is the thickness parameter, Nb is the Brownian motion

parameter and Nt is the thermophoresis parameter. The following expressions are obtained:

$$\lambda = \frac{Re_x \lambda_1 \nu}{2l^2}, Pr = \frac{\nu}{\alpha}, Sc = \frac{\nu}{D_B}, Nb = \frac{\tau D_B}{\nu} C_0 V(\frac{x}{2}), Nt = \frac{\tau D_T}{\nu T_\infty} T_0 V(\frac{x}{2}), \tag{17}$$

where the primes denote the differentiation with respect to the similarity variable ξ. The quantities of practical interest are the local Nusselt number Nu_x and the local Sherwood number Sh_x, which are defined as

$$Nu_x = \frac{x q_w}{k(T_w - T_\infty)}, Sh_x = \frac{x q_m}{D_B(C_w - C_\infty)}, \tag{18}$$

q_w is the heat flux and q_m is the mass flux, which are given by

$$q_w = -k\left(\frac{\partial T}{\partial y}\right)\Big|_{y=ae^{-\frac{nx}{2l}}}, q_m = -D_B\left(\frac{\partial C}{\partial y}\right)\Big|_{y=ae^{-\frac{nx}{2l}}}. \tag{19}$$

The local Nusselt number Nu_x and the local Sherwood number Sh_x are obtained as

$$Nu_x = -Re_x^{1/2}\frac{x}{2l}\theta'(0), Sh_x = -Re_x^{1/2}\frac{x}{2l}\phi'(0), \tag{20}$$

where $Re_x = 2lu_0 e^{nx/l}/\nu$ is the local Reynolds number.

4. Results and Discussions

In this paper, the steady flow of Maxwell nanofluid over an exponential stretching sheet with variable thickness is studied analytically. The ordinary differential Eqs. (12)-(14), subject to the boundary conditions (16) are solved using HAM. The effects of various physical parameters, such as shape parameter n, thickness parameter β, Brownian motion parameter Nb and thermophoresis parameter Nt are interpreted graphically on velocity, thermal and nanoparticles concentration fields. Then the variations of local Nusselt number Nu_x and local Sherwood number Sh_x are examined with respect to shape parameter n and thickness parameter β.

4.1. Convergence of the series solutions for HAM

The governing non-linear similarity equations and their boundary conditions (12)-(16) are solved by HAM analytically. It is straightforward to use the set of base functions:

$$\{\exp(-i\xi)|i \geq 0\}. \tag{21}$$

Base on the rule of solution expressions (21) and the boundary conditions (15)-(16), the following initial guesses for functions f, θ and ϕ are chosen as follows

$$f_0(\xi) = -\beta + 1 - e^{-\xi}, \theta_0(\xi) = e^{-\xi}, \phi_0(\xi) = e^{-\xi}. \tag{22}$$

$\hbar$ curves (10th order HAM solutions for velocity, temperature and nanoparticle volume fraction profiles, respectively) are shown in Fig. 2 at $\lambda = 1, n = 1, \beta = 1, Pr = 1, Nb = 0.1, Nt = 0.1$ and $Sc = 2$. It is clearly noted from Fig. 2 that the admissible values of $\hbar_f$ is $-1.75 < \hbar_f < -0.1$, the admissible values of $\hbar_\theta$ is $-1.6 < \hbar_\theta < -0.8$ and the admissible values of $\hbar_\phi$ is $-1.45 < \hbar_\phi < -0.2$. Accordingly, the better convergent values can be taken within the close range of $-1.45 < \hbar < -0.8$ in conventional HAM. Futhermore, Table 1 shows local Nusselt number and local Sherwood number for different Pr by HAM in comparison to the numerical solution by BVP4C function in Matlab. From Table 1, one can see a very good agreement between the analytic results of HAM and numerical results.

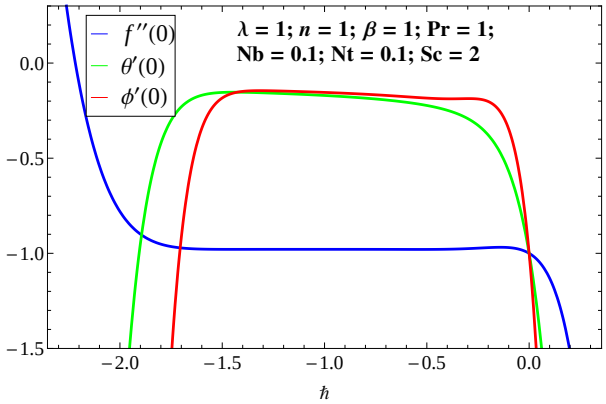

Fig. 2: The $\hbar$ curves of $f''(0)$, $\theta'(0)$, $\phi'(0)$ for the 10th-order approximation solutions.

Table 1: Comparison between the HAM and the BVP4C for local Nusselt number Nu_x and local Sherwood number Sh_x at $\hbar = -1.4$.

	local Nu_x		local Sh_x	
Pr	HAM	BVP4C	HAM	BVP4C
1.0	0.153557	0.1535547	0.148857	0.148815
1.5	0.118046	0.1180443	0.167778	0.167778
2.0	0.087897	0.0878968	0.187639	0.185647
2.5	0.062327	0.0623247	0.203694	0.203739
3.0	0.040292	0.0403114	0.217337	0.217264

4.2. Analysis of the thickness parameter and the shape parameter

Figs. 3–5 depict the effects of thickness parameter β and shape parameter n on the distribution of velocity $f'(\xi)$ and temperature $\theta(\xi)$ for Maxwell nanofluid. As shown in Fig. 3, the velocity distribution and boundary layer thickness increase with higher thickness parameter. Since wall thickness parameter is increased, the stretching velocity enhances which leads to flow velocity enhancement. The effects of the thickness parameter β on the temperature profile are illustrated in Fig. 4. The temperature increases and the thickness of thermal boundary layer becomes thicker as the thickness parameter is lengthened. That's because the temperature on the wall becomes larger with the increase of thickness parameter, in other words, that the wider range of temperature increases between the surface of sheet and ambient fluid, which causes a enhancement in temperature. The influence of shape parameter n on velocity is depicted in Fig. 5. It is presented that the velocity decreases in the boundary layer for each of the shape parameter, which results in a thinner boundary layer. Table 2 shows the results of local Nusselt number, local Sherwood number and velocity gradient at the sheet surface corresponding to different values of β and n with the set of parameters $\lambda = 1, Nb = 0.1, Nt = 0.1, Pr = 1, Sc = 2$. It can be observed from Table 2 that the local Nusselt number and the Sherwood number decay by increase of the shape parameter n, while the opposite trend is

observed for the values of velocity gradient at the sheet surface.

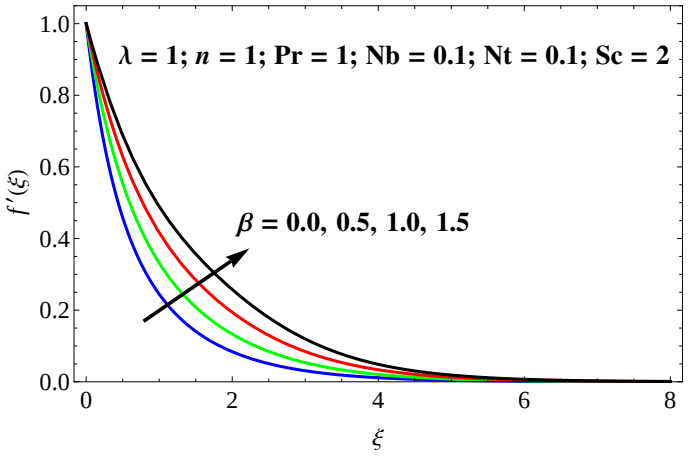

Fig. 3: Change of velocity profile $f'(\xi)$ for different values of β.

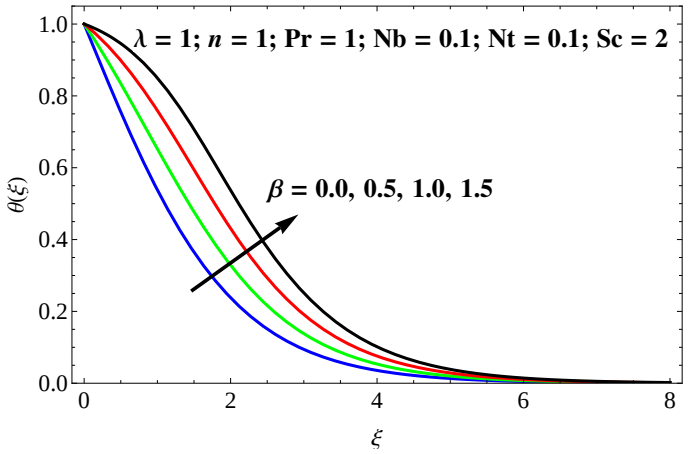

Fig. 4: Change of temperature profile $\theta(\xi)$ for different values of β.

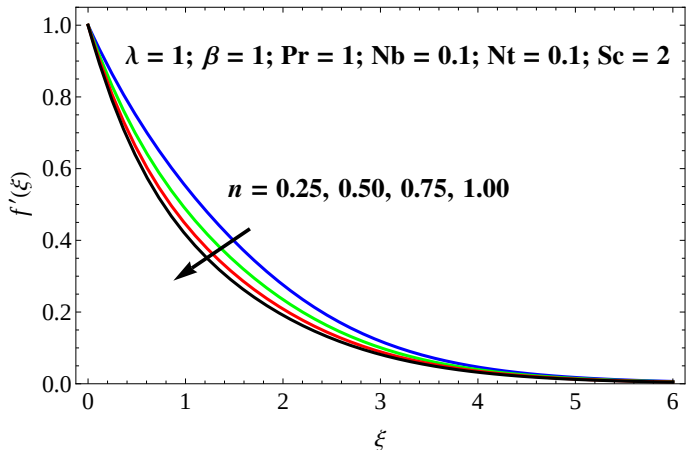

Fig. 5: Change of velocity profile $f'(\xi)$ for different values of n.

Table 2: $-\theta'(0)$, $-\phi'(0)$ and $-f''(0)$ distributions for different values of β and n when $\lambda = 1, Nb = 0.1, Nt = 0.1, Pr = 1, Sc = 2$.

β	n	$-\theta'(0)$	$-\phi'(0)$	$-f''(0)$
0.5	0.5	0.308866	0.298822	0.912006
	0.75	0.301025	0.297178	1.11429
	1.0	0.287039	0.282183	1.13996
1.0	0.5	0.223845	0.206142	0.768012
	0.75	0.186553	0.175544	0.891715
	1.0	0.153557	0.148857	0.979111

4.3. Analysis of the Brownian motion parameter and the thermophoresis parameter

Fig. 6 displays the effects of Brownian motion parameter on temperature distribution of nanofluid. The results show the temperature profiles of nanofluid is increased by Brownian motion parameter. This is because the influence of heat conduction penetrate farther into the fluid with enhanced random motion of nanoparticles. Consequently the thermal boundary layer becomes thicker, which implies a lower efficiency of convection thermal transport.

Fig. 7 (a)-(b) illustrate the influence of therophoresis parameter Nt on the distribution of nanoparticle volume fraction. When $\beta = 0$, i.e. reduced to the flat sheet case, as presented in Fig. 7 (a), one can observe that the volume fraction distribution of nanoparticles increases uniformly in the whole concentration boundary layer for higher therophoresis parameter Nt. Physically there would be an increase of mass boundary layer thickness with the accretion of thermophoretic force, which leads to transfer nanoparticles towards cold regions and thus boosts the magnitude of nanoparticle volume fraction profile. Fig. 7 (b) presents the nanoparticle volume fraction profile for the thickness parameter $\beta = 1$. The nanoparticle volume fraction distribution decreases with the increasing therophoresis parameter near the surface, but the opposite trend occurs far away from the surface. This due to the fact that the variable thickness sheet facilitates the convection transfer of nanoparticles. Another point worthy of comment is that the thickness of nanoparticle volume fraction boundary layer rises with increasing Nt and the distribution of nanoparticle volume fraction is similar to the case with the flat sheet as shown in Fig. 7 (a) for the zone of far away from the surface.

By further calculation, a pretty interesting result is observed: there exists a critical value of the thickness parameter β_c ($\beta_c \approx 0.7$) for the occurrence of intersection point in the profile of nanoparticle volume fraction under the change of therophoresis parameter Nt. As presented in Fig. 7, the nanoparticle volume fraction in the boundary layer has different variable trend on different side of the critical value β_c. That is to say, the nanoparticle volume fraction profile ϕ enhances with the increase of Nt in the whole layer when the thickness parameter is less than the critical point ($\beta < \beta_c$). For $\beta > \beta_c$, there appears an intersection point as seen in Fig. 7 (b). What's more, the position of the intersection point is gradually far away from the stretching sheet with increasing β. As is well known, the Sherwood number Sh_x is a measurement of mass transfer. Fig. 8 illustrates results of local Sherwood number for different thickness number β. The local Sherwood number enlarges with increasing the thickness parameter when the therophoresis diffusion has dominant effects in mass trans-

fer (the thickness parameter below the critical value $\beta < \beta_c$). This due to the fact that thermophoretic diffusion enhances the mass transfer of nanoparticles in Maxwell fluid, thus the local Sherwood number is higher. However, There is a reduction in the local Sherwood number with thickness parameter accretion as the thickness parameter has dominant effects (the thickness parameter upon the critical value $\beta > \beta_c$). Moreover, at the critical value $\beta_c \approx 0.7$ the ability of mass transfer achieves the highest value.

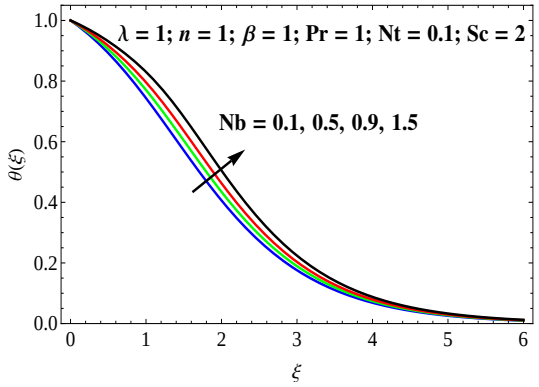

Fig. 6: Change of temperature profile $\theta(\xi)$ for different values of Nb.

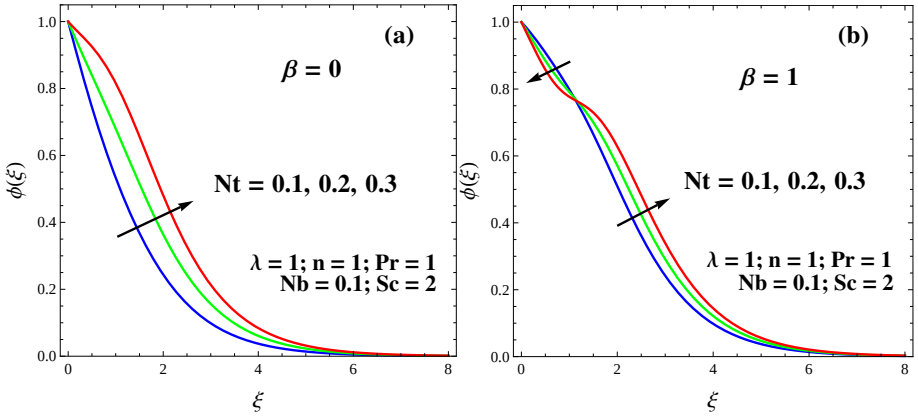

Fig. 7: Change of nanoparticle volume fraction profile $\phi(\xi)$ of different thickness parameter β for different values of Nt. (a) $\beta = 0$; (b) $\beta = 1$.

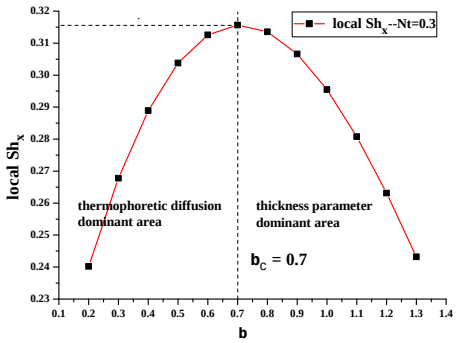

Fig. 8: Local Sherwood number Sh_x for various values of β with condition $\lambda = 1, n = 1, Pr = 1, Sc = 2, Nb = 0.1, Nt = 0.3$.

4.4. Analysis of the local Nusselt number and the local Sherwood number

The variations of heat transfer rate and mass transfer rate for various values of sheet shape parameter are investigated. Fig. 9 (a) describes variation in local Nusselt number with an increase in shape parameter n for different values of Pr. It can be seen that heat transfer rate at the stretching sheet decreases when the shape parameter is increased. This is due to the fact that the temperature of surface becomes larger as n increases. Further the thermal boundary layer thickness increases and the thermal resistance becomes stronger. Fig. 9 (b) illustrates the variation of local Sherwood number with the sheet shape parameter for different values of Schmidt number. The increase of shape parameter leads to the decrease of the mass transfer on the sheet. It is also important that the rate of decline for local Nusselt number becomes larger with increase of the Schmidt number. The effects of the thickness parameter β on local Nusselt number and local Sherwood number are presented in Fig. 10. One can conclude from Fig. 10 (a) and (b) that the increase of the thickness parameter causes the reduction of heat transfer on the sheet surface (decrease of local Nusselt number) and mass transfer of nanoparticles (decrease of local Sherwood number). Because larger thickness parameter means thicker thermal boundary layer and higher thermal resistance, which finally results in lower heat transfer on sheet surface. Mass transfer of nanoparticles is similar to heat transfer on the sheet surface.

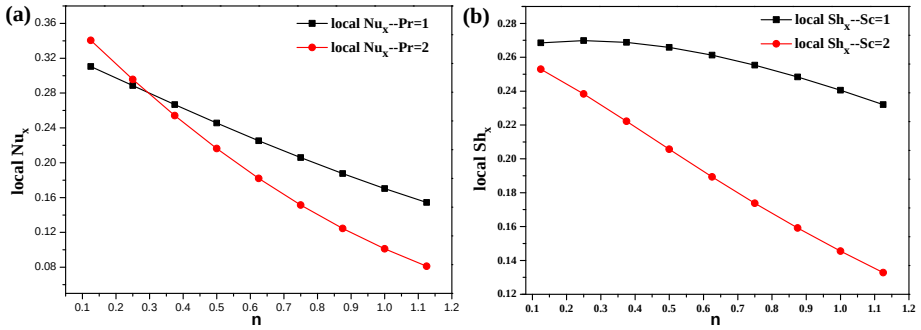

Fig. 9: Local Nusselt number Nu_x with conditions $Pr = 1, 2$ and local Sherwood number Sh_x with conditions $Sc = 1, 2$ for various values of n as $\lambda = 1, \beta = 1, Nb = 0.1, Nt = 0.1$.

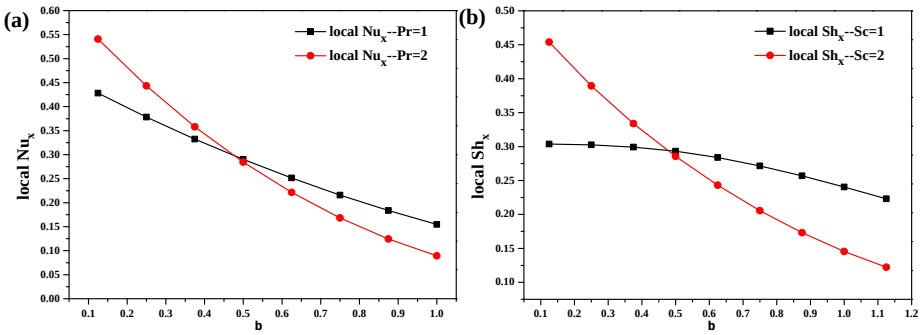

Fig. 10: Local Nusselt number Nu_x with conditions $Pr = 1, 2$ and local Sherwood number Sh_x with conditions $Sc = 1, 2$ for various values of β as $\lambda = 1, \beta = 1, Nb = 0.1, Nt = 0.1$.

5. Conclusions

The effects of variable thickness stretching sheet on heat and mass transfer for nanofluid in boundary layer flow has been investigated. The two-component Buongiorno model is utilized in the mathematical formulation to describe the motion of nanoparticles. Approximate solutions are obtained by HAM and these results are in good agreement with the numerical solutions. Several important conclusions are as follows:

(I) Thickness parameter has significant effects on the velocity, temperature fields and the local Nusselt number. As thickness parameter increases,

local Nusselt number decreases, while the velocity and temperature profiles increase.

(II) Shape parameter of stretching sheet strongly affects the velocity fields and the local Nusselt number. As the shape parameter increases, both velocity and local Nusselt number decrease.

(III) There appears a critical value of the thickness parameter, at which the nanoparticle volume fraction profile has different distribution on the different side of the critical value ($\beta_c \approx 0.7$). For $\beta < \beta_c$, the variation of nanoparticle volume fraction distribution with increasing therophoresis parameter is similar to the plate model. For $\beta > \beta_c$, the nanoparticle volume fraction distribution decreases with increasing therophoresis parameter near the surface, but the opposite trend occurs far away from the surface.

(IV) The variation of the local Sherwood number are not necessarily monotonic with thickness parameter β as showed in Fig. 8. In monotone variation situation such as $Nt = 0.1$, the local Sherwood number decreases with increasing the shape parameter and thickness parameter.

Nomenclature

a	variable thickness parameter, [m]
C	nanoparticle volume fraction, $[kg\ m^{-3}]$
C_0	reference nanoparticle volume fraction, $[kg\ m^{-3}]$
C_w	nanoparticle volume fraction at stretching surface, $[kg\ m^{-3}]$
C_∞	ambient nanoparticle, $[kg\ m^{-3}]$
D_B	Brownian diffusion coefficient, $[m^2\ s^{-1}]$
D_T	thermophoretic diffusion coefficient, $[m^2\ s^{-1}]$
f	similar stream function, $[-]$
k	thermal conductivity, $[Wm^{-1}\ K]$
l	reference length, $[m]$
Nb	Brownian motion parameter, $[-]$
Nt	thermophoresis parameter, $[-]$
Nu_x	local Nusselt number, $[-]$
n	shape parameter, $(n > 0)$, $[-]$
Pr	Prandtl number, $[-]$
q_m	wall mass flux, $[kg\ m^{-2}s^{-1}]$
q_w	wall heat flux, $[W\ m^{-2}]$
Re_x	local Reynolds number, $[-]$
Sc	Schmidt number, $[-]$
Sh_x	local Sherwood number, $[-]$
T	temperature of fluid, $[K]$
T_0	reference temperature, $[K]$
T_w	sheet surface temperature, $[K]$
T_∞	ambient temperature, $[K]$

u,v	velocity in x,y-axis direction, $[m\ s^{-1}]$
u_0	reference velocity, $[m\ s^{-1}]$
U_w	stretching sheet velocity, $[m\ s^{-1}]$
x,y	x,y-axis, $[m]$
Greek symbols	
α	thermal diffusivity, $[m^2\ s^{-1}]$
β	surface thickness parameter, $[-]$
η	similarity variable, $[-]$
ξ	similarity variable after coordinate transformation, $[-]$
θ	dimensionless variable of T, $[-]$
ϕ	dimensionless variable of C, $[-]$
ψ	stream function, $[m^2\ s^{-1}]$
λ	local Deborah number, $(\lambda > 0)$, $[-]$
λ_1	relaxation time, $[s]$
ν	kinematic viscosity, $[m^2\ s^{-1}]$
$(\rho c_p)_f$	heat capacity of fluid, $[kg\ m^{-3}K]$
$(\rho c_p)_p$	heat capacity of nanoparticle, $[kg\ m^{-3}K]$
τ	nanoparticle heat capacity ratio, $[-]$
Subscripts	
w	condition at the surface, $[-]$
∞	ambient condition, $[-]$
c	critical value, $[-]$
f	fluid, $[-]$
p	pressure, $[-]$
Superscripts	
$'$	differentiation with respect to η or ξ, $[-]$

Acknowledgments

This work was supported by the National Natural Science Foundation of China (Grant Nos.11772046, 11771040).

References

[1] W. H. Azmi, K. V. Sharma, R. Mamat, G. Najafi, M. S. Mohamad, The enhancement of effective thermal conductivity and effective dynamic viscosity of nanofluids-A review, Renewable & Sustainable Energy Reviews 53 (2016) 1046–1058.

[2] M. R. Eid, Time-Dependent Flow of Water-NPs Over a Stretching Sheet in a Saturated Porous Medium in the Stagnation-Point Region in the Presence of Chemical Reaction, Journal of Nanofluids 6 (3) (2017) 550–557.

[3] M. R. Eid, A. Alsaedi, T. Muhammad, T. Hayat, Comprehensive analysis of heat transfer of gold-blood nanofluid (Sisko-model) with thermal radiation, Results in Physics.

[4] J. Buongiorno, Convective transport in nanofluids, Journal of Heat Transfer 128 (3) (2006) 240–250. doi:10.1115/1.2150834.

[5] C. Yang, Q. Wang, A. Nakayama, T. Qiu, Effect of temperature jump on forced convective transport of nanofluids in the continuum flow and slip flow regimes, Chemical Engineering Science 137 (2015) 730–739.

[6] R. U. Haq, S. Nadeem, Z. H. Khan, N. S. Akbar, Thermal radiation and slip effects on MHD stagnation point flow of nanofluid over a stretching sheet, Physica E: Low-dimensional Systems and Nanostructures 65 (2015) 17–23.

[7] M. R. Eid, Chemical reaction effect on MHD boundary-layer flow of two-phase nanofluid model over an exponentially stretching sheet with a heat generation, Journal of Molecular Liquids 220 (2016) 718–725.

[8] M. Narahari, S. S. K. Raju, R. Pendyala, Unsteady natural convection flow of multi-phase nanofluid past a vertical plate with constant heat flux, Chemical Engineering Science 167 (2017) 229–241.

[9] M. R. Eid, K. L. Mahny, Flow and heat transfer in a porous medium saturated with a Sisko nanofluid over a nonlinearly stretching sheet with heat generation/absorption, Heat TransferAsian Research.

[10] A. Kuznetsov, D. Nield, Natural convective boundary-layer flow of a nanofluid past a vertical plate, International Journal of Thermal Sciences 49 (2) (2010) 243–247. doi:10.1016/j.ijthermalsci.2009.07.015.

[11] M. Sheikholeslami, M. Gorji-Bandpy, D. Ganji, P. Rana, S. Soleimani, Magnetohydrodynamic free convection of Al2O3–water nanofluid considering thermophoresis and Brownian motion effects, Computers & Fluids 94 (2014) 147–160. doi:10.1016/j.compfluid.2014.01.036.

[12] M. R. Eid, K. L. Mahny, Unsteady MHD heat and mass transfer of a non-Newtonian nanofluid flow of a two-phase model over a permeable stretching wall with heat generation/absorption, Advanced Powder Technology.

[13] S. Nadeem, R. U. Haq, Z. Khan, Numerical study of MHD boundary layer flow of a Maxwell fluid past a stretching sheet in the presence of nanoparticles, Journal of the Taiwan Institute of Chemical Engineers 45 (1) (2014) 121–126. doi:10.1016/j.jtice.2013.04.006.

[14] R. Kandasamy, C. Jeyabalan, K. S. Prabhu, Nanoparticle volume fraction with heat and mass transfer on MHD mixed convection flow in a nanofluid in the presence of thermo-diffusion under convective boundary condition, Applied Nanoscience 6 (2) (2016) 287–300. doi:10.1007/s13204-015-0435-5.

[15] S. U. Rehman, R. U. Haq, Z. H. Khan, C. Lee, Entropy generation analysis for non-Newtonian nanofluid with zero normal flux of nanoparticles at the stretching surface, Journal of the Taiwan Institute of Chemical Engineers 63 (2016) 226–235.

[16] M. Atlas, R. U. Haq, T. Mekkaoui, Active and zero flux of nanoparti-

cles between a squeezing channel with thermal radiation effects, Journal of Molecular Liquids 223 (2016) 289–298.

[17] F. A. Soomro, R. U. Haq, Z. H. Khan, Q. Zhang, Passive control of nanoparticle due to convective heat transfer of prandtl fluid model at the stretching surface, Chinese Journal of Physics.

[18] D. Rollins, K. Vajravelu, Heat transfer in a second-order fluid over a continuous stretching surface, Acta mechanica 89 (1991) 167–178. doi:10.1007/BF01171253.

[19] W. Khan, I. Pop, Boundary-layer flow of a nanofluid past a stretching sheet, International Journal of Heat and Mass Transfer 53 (11) (2010) 2477–2483. doi:10.1016/j.ijheatmasstransfer.2010.01.032.

[20] O. D. Makinde, A. Aziz, Boundary layer flow of a nanofluid past a stretching sheet with a convective boundary condition, International Journal of Thermal Sciences 50 (7) (2011) 1326–1332.

[21] M. E. Ali, On thermal boundary layer on a power-law stretched surface with suction or injection, International Journal of Heat and Fluid Flow 16 (4) (1995) 280–290. doi:10.1016/0142-727X(95)00001-7.

[22] E. Magyari, B. Keller, Heat and mass transfer in the boundary layers on an exponentially stretching continuous surface, Journal of Physics D: Applied Physics 32 (5) (1999) 577. doi:10.1088/0022-3727/32/5/012.

[23] T. Fang, J. Zhang, Y. Zhong, Boundary layer flow over a stretching sheet with variable thickness, Applied Mathematics and Computation 218 (13) (2012) 7241–7252. doi:10.1016/j.amc.2011.12.094.

[24] T. Hayat, M. I. Khan, M. Farooq, A. Alsaedi, M. Waqas, T. Yasmeen, Impact of Cattaneo–Christov heat flux model in flow of variable thermal conductivity fluid over a variable thicked surface, International Journal of Heat and Mass Transfer 99 (2016) 702–710. doi:10.1016/j.ijheatmasstransfer.2016.04.016.

[25] M. Abdel-Wahed, E. Elbashbeshy, T. Emam, Flow and heat transfer over a moving surface with non-linear velocity and variable thickness in a nanofluids in the presence of Brownian motion, Applied Mathematics and Computation 254 (2015) 49–62. doi:10.1016/j.amc.2014.12.087.

[26] T. Salahuddin, M. Malik, A. Hussain, S. Bilal, M. Awais, mhd flow of cattanneo–christov heat flux model for williamson fluid over a stretching sheet with variable thickness: using numerical approach, Journal of magnetism and magnetic materials 401 (2016) 991–997. doi:10.1016/j.jmmm.2015.11.022.

[27] K. Prasad, K. Vajravelu, H. Vaidya, Hall effect on MHD flow and heat transfer over a stretching sheet with variable thickness, International Journal for Computational Methods in Engineering Science and Mechanics 17 (4) (2016) 288–297. doi:10.1080/15502287.2016.1209795.

[28] K. Sadeghy, A.-H. Najafi, M. Saffaripour, Sakiadis flow of an upper-convected Maxwell fluid, International Journal of Non-Linear Mechanics 40 (9) (2005) 1220–1228. doi:10.1016/j.ijnonlinmec.2005.05.006.

[29] T. Hayat, C. Fetecau, Z. Abbas, N. Ali, Flow of a Maxwell fluid between two side walls due to a suddenly moved plate, Nonlinear Analysis: Real World Applications 9 (5) (2008) 2288–2295. doi:10.1016/j.nonrwa.2007.08.005.

[30] V. Singh, S. Agarwal, Flow and heat transfer of Maxwell fluid with variable viscosity and thermal conductivity over an exponentially stretching sheet, American journal of fluid dynamics 3 (4) (2013) 87–95. doi:10.5923/j.ajfd.20130304.01.

[31] K.-L. Hsiao, Combined electrical MHD heat transfer thermal extrusion system using Maxwell fluid with radiative and viscous dissipation effects, Applied Thermal Engineering 112 (2016) 1281–1288. doi:10.1016/j.applthermaleng.2016.08.208.

[32] N. Khan, T. Mahmood, M. Sajid, M. S. Hashmi, Heat and mass transfer on MHD mixed convection axisymmetric chemically reactive flow of Maxwell fluid driven by exothermal and isothermal stretching disks, International Journal of Heat and Mass Transfer 92 (2016) 1090–1105. doi:10.1016/j.ijheatmasstransfer.2015.09.001.

[33] M. Mustafa, T. Hayat, A. Alsaedi, Rotating flow of Maxwell fluid with variable thermal conductivity: An application to non-Fourier heat flux theory, International Journal of Heat and Mass Transfer 106 (2017) 142–148. doi:10.1016/j.ijheatmasstransfer.2016.10.051.

[34] N. A. Halim, R. U. Haq, N. F. M. Noor, Active and passive controls of nanoparticles in Maxwell stagnation point flow over a slipped stretched surface, Meccanica (2017) 1–13.

[35] S. Liao, The proposed homotopy analysis technique for the solution of nonlinear problems, Ph.D. thesis, Shanghai Jiao Tong University (1992).

[36] S. Liao, Beyond perturbation: introduction to the homotopy analysis method, CRC press, Boca Raton, 2003.

[37] M. Rashidi, S. Abbasbandy, et al., Analytic approximate solutions for heat transfer of a micropolar fluid through a porous medium with radiation, Communications in Nonlinear Science and Numerical Simulation 16 (4) (2011) 1874–1889. doi:10.1016/j.cnsns.2010.08.016.

[38] M. Turkyilmazoglu, A note on the homotopy analysis method, Applied Mathematics Letters 23 (10) (2010) 1226–1230. doi:10.1016/j.aml.2010.06.003.

[39] M. M. Rashidi, E. Momoniat, B. Rostami, Analytic approximate solutions for MHD boundary-layer viscoelastic fluid flow over continuously moving stretching surface by homotopy analysis method with two auxiliary parameters, Journal of Applied Mathematics 2012 (11) (2012) 853–862. doi:10.1155/2012/780415.

[40] C. Liu, M. Pan, L. Zheng, C. Ming, X. Zhang, Flow and Heat Transfer of Bingham Plastic Fluid over a Rotating Disk with Variable Thickness, Zeitschrift für Naturforschung A 71 (11) (2016) 1003–1015. doi:10.1515/zna-2016-0218.

[41] C. Zhang, L. Zheng, X. Zhang, G. Chen, MHD flow and radiation heat transfer of nanofluids in porous media with variable surface heat flux and chemical reaction, Applied Mathematical Modelling 39 (1) (2015) 165–181. doi:10.1016/j.apm.2014.05.023.

[42] R. U. Haq, P. Bestapu, S. Bandari, Q. M. Al-Mdallal, Mixed Convection Flow of Thermally Stratified MHD Nanofluid over an Exponentially Stretching Surface with Viscous Dissipation Effect, Journal of the Taiwan Institute of Chemical Engineers 71.